Noname manuscript No.
(will be inserted by the editor)

New topologies in the unfolding of the Doubly Degenerate Bogdanov-Takens singularity

Marisa Saggio

Received: date / Accepted: date

Abstract High-codimension bifurcations play a key role in shaping the dynamics of nonlinear models, as their unfoldings establish structured relationships between lower-codimension bifurcations and, ultimately, the attractors they generate. Owing to this unifying and predictive capacity, such bifurcations are attracting growing interest in mathematical biology, particularly in neuroscience. One notable example is the codimension-3 Degenerate Bogdanov-Takens (DBT) singularity, proposed as an organizing center for neural dynamics at both the single-neuron and population levels and playing a key role in bursting. The DBT itself arises within the unfolding of an even higher-order singularity, the Doubly Degenerate Bogdanov-Takens (DDBT), whose structure remains only partially understood, despite initial indications of its relevance in systems exhibiting a DBT singularity. Here, we contribute by employing numerical continuation to explore the DDBT unfolding using spheres in parameter space. We confirm the conjecture that it connects DBT to another highly symmetric codimension-3 bifurcation, but through transitions that differ in part from those previously proposed in the literature, with one intermediate passage remaining unclear. We also show that using planes, rather than spheres, to explore the unfolding allows for additional bifurcation topologies. Overall, the intermediate configurations and additional bifurcation structures reveal a rich repertoire of dynamical behaviors that improve our understanding of what models with a DDBT point can do and how these behaviors are related. We draw on neuroscience for examples of these topologies in models of neural dynamics.

Keywords High-codimension bifurcations · Unfolding of singularities · Codimension-four Bogdanov-Takens · Neural dynamics · Organizing centers

This research has received funding from the European Union's Horizon Europe Programme under the Specific Grant Agreement No. 101147319 (EBRAINS 2.0 Project).

Marisa Saggio
Aix Marseille Univ, INSERM, INS, Inst Neurosci Syst, Marseille, France
Orcid: 0000-0002-3846-6100
E-mail: maria-luisa.saggio@univ-amu.fr

1 Introduction

When describing a system using differential equations, we often focus on the stable configurations it eventually settles into: the *attractors* of the dynamics. As system parameters change, these attractors can appear, disappear, or switch stability. This qualitative transformation of the attractor landscape is known as a *bifurcation*, and a bifurcation diagram depicts these changes under parameter variation. Parameters may represent, for example, internal properties or external conditions. Common bifurcations in planar systems (Fig. 1A), such as Fold (F), Hopf (H), Homoclinic (Hom), Fold of Limit Cycle (FLC) or Saddle-Node-on-Invariant-Circle (SNIC) require the variation of one parameter, and are thus called *codimension-1* (cod-1) bifurcations. If the system involves more parameters, we can study how cod-1 bifurcations depend on them, creating higher-dimensional bifurcation diagrams. For example, in a two-parameter bifurcation diagram, cod-1 bifurcations appear as curves, stratifying the space into regions within which the repertoire of available behaviors stays *qualitatively* the same (Fig. 1B). Bifurcation diagrams, thus, provide condensed information about what a system can do and how this varies with parameter values [28].

Cod-1 bifurcations in two-parameter diagrams cannot occur in arbitrary configurations. Instead, they are arranged in characteristic ways, locally organized by *codimension-2* (cod-2) bifurcations, that is, bifurcations requiring the precise tuning of two parameters. At a cod-2 bifurcation, two or more bifurcations coincide. Moving away in parameter space from the cod-2 point, cod-1 curves unfold from it stereotypically, as described by the *unfolding* of that specific cod-2 bifurcation. Some examples are shown in Fig. 1B.

The configurations of cod-2 bifurcations themselves can be organized by the unfoldings of cod-3 bifurcations, and so on. This implies that high-codimension bifurcations, far from being esoteric mathematical objects [27], act as organizing centers that unify a system's behaviors through their unfoldings [17,26,27]. High-codimension bifurcations are the reason for which "there are some two-dimensional bifurcation diagrams of planar vector fields that seem to have a *universal character* in the sense that they occur in many models" [25]. Knowing that a system possesses a high-codimension singularity is therefore a compact yet powerful source of information about its possible dynamics, from lower-order bifurcations down to attractors and repellors. Recognizing in a two-parameter bifurcation diagram the signatures of a high-codimension singularity, on the other hand, can immediately reveal other bifurcation topologies that can be expected if parameters are varied.

While many cod-1 and cod-2 bifurcations and their unfoldings are described in textbooks [28], this is rarely the case for higher-order bifurcations, which are only partially understood.

Among them, the Degenerate Bogdanov-Takens (DBT) singularity, focus case [14,29], is a well-studied codimension-3 bifurcation that appears in applications including ecology [4,28], chemistry [9,10] and neural dynamics. In neuroscience, is present in several single neuron models [20,1]. In particular, it has been proven to occur in any conductance-based model for Type I excitability [26,31,40,15,16,35,12,34,18].

DBT has been proposed as an organizing center for the activity of single neurons [33,26] and, possibly, for neural population dynamics [37,36]. When coupled with slow variables to form a *fast–slow system*, it can produce several classes of bursting, some of which are observed in specific types of excitable cells [6,19,33,36].

This cod-3 bifurcation is itself part of the unfolding of the cod-4 Doubly Degenerate Bogdanov-Takens singularity (DDBT), whose structure remains not completely understood [25]. Notably, Osinga and colleagues showed that a portion of the DDBT unfolding they investigated supports fold/subH bursting (bursting with a fold bifurcation at the onset of oscillations and a subH at their offset [21]) observed in some excitable cells, and explains its proximity to the more common fold/Hom bursting [33]. This led the authors to propose the DDBT, rather than simply the DBT, as an organizing center for excitable cells' dynamics. The unfolding-theory approach to fast–slow bursting [19] was later systematically applied to this explored portion of the DDBT unfolding in [36]. This analysis demonstrated that all sixteen theoretically possible planar point-cycle bursters from Izhikevich classification [21] can be represented within this unfolding when independently oscillating slow variables are involved (*slow-wave bursting*), and all except two when the slow variable relies on feedback from fast ones to oscillate (*hysteresis-loop bursting*).

The case in which b, the fourth parameter of the unfolding of the DDBT, is equal to 0 has been studied in detail [25]. This gives a reflectionally symmetric bifurcation structure found in models of electrical circuits, in chemistry, biochemistry and ecology [3,24,39, 7,5,30,25]. On the other hand, the bifurcation structure of the unfolding of DBT occurs for large values of b. In 1998, Khibnik and colleagues conjectured a number of intermediate bifurcation diagrams which modify

Table 1 List of abbreviations.

Abbr.	Meaning and alternative names
Solutions	
FP	Fixed Point
LC	Limit Cycle
NS	Neutral-Saddle
Codimension-1	
F	Fold (Saddle-Node, Limit-Point)
SNIC	Saddle-Node on Invariant Circle
Hom	Homoclinic (Saddle-Homoclinic, Loop)
H	Hopf
FLC	Fold Limit Cycle (Limit Point of Cycles, Double Limit Cycle)
Codimension-2	
C	Cusp
BT	Bogdanov-Takens
B	Bautin (gen. Hopf)
SNL	Saddle-Node Loop (Saddle-Node-Homoclinic)
DL	Deg. Loop (Neutral-Saddle Loop, resonant Homoclinic)
Codimension-3 and 4	
DBT	Deg. Bogdanov-Takens - here, focus case (Bogdanov-Takens-Cusp, nilpotent Cusp of order three, cubic BT)
DDBT	Doubly Deg. Bogdanov-Takens
Other	
sub/sup	subcritical / supercritical
gen.	generalized
deg.	degenerate

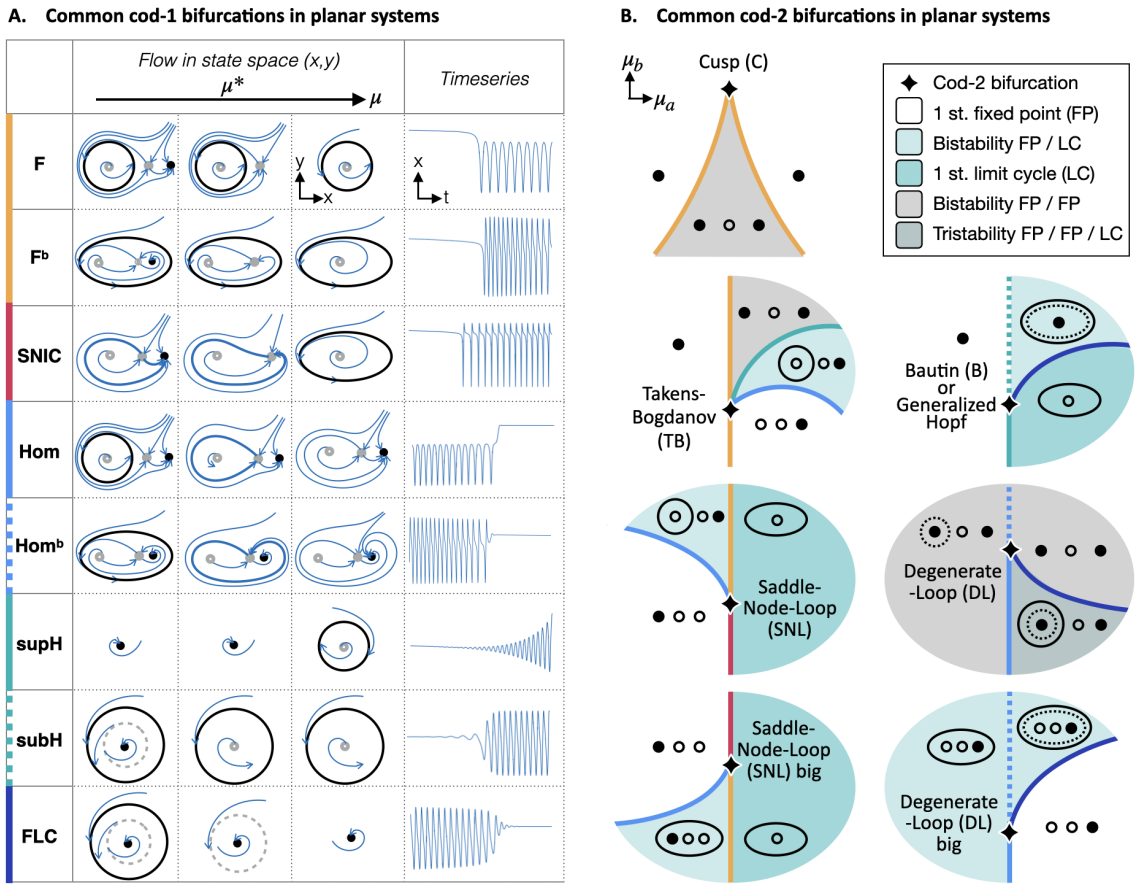

Fig. 1 Some common cod-1 and cod-2 bifurcations in dynamical systems. A. Cod-1 bifurcations (abbreviations in Table 1) involving stable/unstable fixed points for fixed solutions (full/empty dots), and stable/unstable limit cycles for oscillatory solutions (full/dashed ellipses). For each bifurcation, we show the color used in this paper, the configuration of attractors (black) and repellors (gray) in state space (x, y) before, at, and after the bifurcation and an example of a timeseries. Trajectories in state space are in blue. Thicker curves identify homoclinic (returning to the same fixed point) and heteroclinic (joining two fixed points) trajectories involved in SNIC and homoclinic bifurcations. The bifurcation occurs at the critical value of the parameter μ^*. At a fold bifurcation, two fixed points coalesce and disappear, and the system settles into a coexisting attractor (in this figure, a limit cycle). At a SNIC, the fold is accompanied by the appearance of a limit cycle. At a homoclinic, a limit cycle meets a saddle and disappears. At a Hopf, the fixed point stability changes and a limit cycle appears. At a FLC, two limit cycles coalesce and disappear. In supercritical and subcritical bifurcations, the new object created is stable and unstable respectively. **B.** Bifurcation diagrams for common cod-2 bifurcations. Cod-1 bifurcation curves stratify the parameter space (μ_a, μ_b). In each region, a possible configuration of attractors and repellors compatible with the curves is shown, as used later in the paper (here, and in the next figures, both attractors and repellors are represented in black). BT and SNL bifurcations can also involve subcritical homoclinic, Hopf and SNIC (not shown). SNL and DL are presented in the two variations used here, with the limit cycle surrounding one or all the fixed points.

the symmetric case leading to the DBT one as b is increased [25]. This sequence is a representation of the unfolding of the cod-4 DDBT. In 2016, Krauskopf and Osinga investigated the cases closer to the DBT case (large b), which differed from those previously conjectured [27]. Given the interest in this singularity and its potential role in neural dynamics [26,1,32,33], but also in other contexts such as cosmology [2] and fusion plasma transport models [11], we here provide a numerical study of other cases from a large enough b down to $b = 0$.

In the remainder of this section, we briefly review the standard approach of using spheres to explore the unfolding of this singularity [14], the DBT and symmetric cases [25], the conjecture about intermediate transitions [25], and the more recent updates [27]. We refer the reader to the original papers for a more in-depth mathematical treatment. In the Results section, we present our numerical explorations and discuss how they relate to the conjecture, identify the newly discovered cases, and highlight which transition remains unclear. We then show that using slices of the unfolding's parameter space, rather than spherical sections, reveals new bifurcation topologies potentially relevant for models in neuroscience and other systems where the DDBT has been identified.

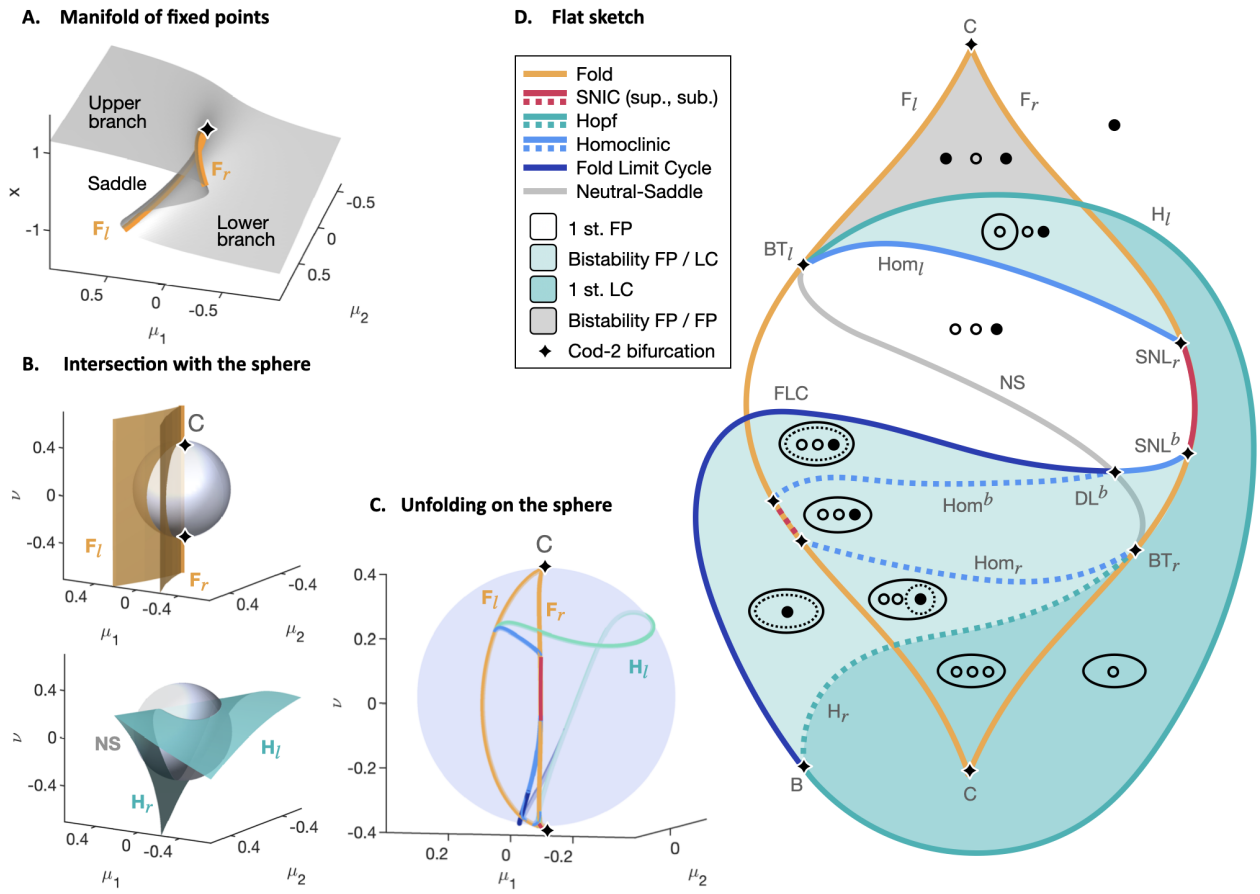

Fig. 2 Unfolding of the degenerate Bogdanov-Takens singularity (DBT) using spherical surfaces ($b = 1$). A. Manifold of fixed points, with cod-1 fold bifurcations meeting at a cod-2 cusp. **B.** Top, intersection between the fold manifold and the spherical surface. Bottom, same for the manifold of Hopf. **C.** Bifurcation diagram on the sphere, including the intersection with the other cod-1 bifurcation manifolds. **D.** Flat topologically equivalent sketch of the bifurcation diagram. A colored background marks the type of attractor in each region. The cod-1 curves are: the fold curves F_l/F_r creating the two leftmost/rightmost fixed points and meeting at two cod-2 C; the Hopf (H) joining two cod-2 BT_l, BT_r, creating or destroying a limit cycle around the leftmost or rightmost fixed point (for convenience in the text, we separated it into two branches H_l and H_r). Homoclinic curves Hom_l/Hom_r are also stemming from the BT points, creating or destroying a limit cycle around the leftmost/rightmost fixed point; Hom^b is responsible for a limit cycle around all three fixed points; FLC stems from a cod-2 B point on the H curve and disappears through a cod-2 DL^b with Hom^b; SNIC curves join either the cod-2 SNL_r and SNL^b points or the analogous points on the left (not labeled because of least interest for this work).

1.1 Equations of the unfolding of the DDBT

The equations for the candidate unfolding for the DDBT proposed in [25] are:

$$\begin{aligned} \dot{x} &= -y \\ \dot{y} &= x^3 - \mu_2 x - \mu_1 - y\left(\nu + bx + x^2\right) \end{aligned} \tag{1}$$

where, as in [14], we consider the parameter space $(-\mu_1, \mu_2, \nu, b)$ and the dot indicates d/dt.

We first highlight which bifurcations can be readily determined to depend on the fourth parameter b.

Fixed points, satisfying $\dot{x}_{fp} = \dot{y}_{fp} = 0$, do not depend on b. A fold bifurcation occurs when two fixed points coalesce. If we consider the Jacobian matrix J of the system computed at its fixed points

$$J_{fp} = \begin{pmatrix} 0 & -1 \\ 3x_{fp}^2 - \mu_2 & -(\nu + bx_{fp} + x_{fp}^2) \end{pmatrix},$$

the manifold of fold bifurcation can be found imposing $\det(J_{fp}) = \lambda_1\lambda_2 = 0$, where $\lambda_{1,2}$ are the eigenvalues of the J_{fp}. This condition implies a zero eigenvalue. In our case, it translates to $3x_{fp}^2 - \mu_2 = 0$, making the fold bifurcation manifold independent of b.

The two surfaces of fold bifurcation meet at $(\mu_1, \mu_2) = (0, 0)$, where $(x_{fp}, y_{fp}) = (0, 0)$. This is the cod-2 Cusp (C) bifurcation where the three branches of fixed points coincide, as shown in Fig. 2A,B top. This is also independent of b.

At a Hopf bifurcation, the fixed point changes stability and a limit cycle is created. To identify the Hopf

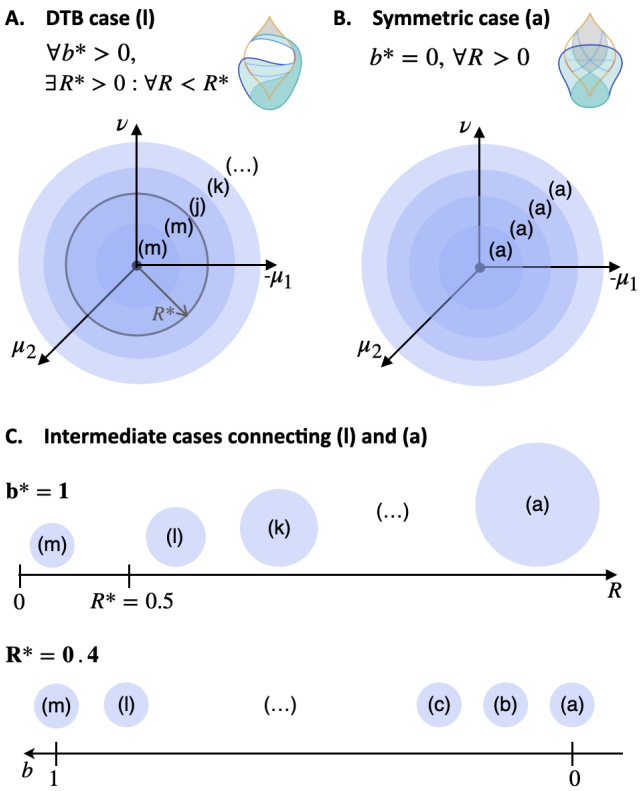

Fig. 3 Exploring the four-dimensional unfolding using spheres with either fixed radius or fixed b. A. Left: the bifurcation diagram of the DBT case (case (m) in this paper) can be found on sufficiently small spheres for any fixed positive value of b. For bigger spheres, the topology of the bifurcation diagram goes through a series of different cases (k, j, ...). Right: when $b = 0$ the symmetric case (a) appears on any sphere. **B.** Top: we can study the sequence of cases connecting (a) to (m) by fixing b and increasing the radius. Alternatively, we can fix the radius and vary b. Values in the figure are those used in this paper.

manifold, we impose $\mathrm{tr}(J_{fp}) = \lambda_1 + \lambda_2 = 0$, this amounts to requiring that the eigenvalues of the fixed point sum to zero. In our case, the condition reads $-(\nu + bx_{fp} + x_{fp}^2) = 0$, which depends on b. It gives the Hopf manifold when the fixed point is not a saddle, i.e.$\det(J_{fp}) > 0$, and the eigenvalues are a purely imaginary pair; it gives instead the Neutral-Saddle (NS) manifold on the saddle solutions, i.e. $\det(J_{fp}) < 0$, where eigenvalues are real and opposite. Neutral-saddle is not a bifurcation, but helps locate cod-2 DL points, as will be explained later.

When both $\det(J_{fp}) = \mathrm{tr}(J_{fp}) = 0$, we have cod-2 Bogdanov-Takens (BT) bifurcations, a double-zero eigenvalue bifurcation, dependent on b because of the condition on the trace. The cod-3 DBT occurs when BT and C coincide, happening for $(\mu_1, \mu_2, \nu) = (0, 0, 0)$ for all values of b.

The bifurcation manifolds mentioned above need to satisfy additional transversality and non-degeneracy conditions. We don't go into the details since our goal in this section is to highlight whether these bifurcations depend on b.

1.2 Using spheres to explore the unfolding

Case $b > 0$ and the unfolding of the DBT

As explained above, for any positive b, a cod-3 DBT is found when the other three parameters are all equal to zero. Moving away from the origin of the $(-\mu_1, \mu_2, \nu)$ space, two-dimensional manifolds of cod-1 bifurcations emerge, with curves of cod-2 bifurcations at some of their intersections. In Fig. 2B top, for example, the orange fold manifolds intersect at a line of cusp bifurcation. While the intersection between fold and Hopf manifolds (Fig. 2B) gives BT curves.

It is not easy to deal with a 3-dimensional space. We can thus consider the intersection between the surface of a sphere centered on the origin (that is, on the DBT singularity) and these manifolds of cod-1 and cod-2 bifurcations (Fig. 2B-C). This provides a two-dimensional bifurcation diagram for each radius $R =$ const, where the angles of the spherical coordinates (θ, ϕ) are the parameters. How useful is this reduced diagram for capturing the unfolding properties? It can be shown [14, 25], that for sufficiently small values of R, the topology of the bifurcation diagram on the sphere (Fig. 2C-D) stays the same, therefore providing an informative representation of the unfolding of the DBT. More precisely, for any value $b^* > 0$ of b, there exists a sufficiently small value of $R = R^*$ such that the same bifurcation topology can be found on any sphere with $R < R^*$, while the topology changes on bigger spheres (Fig. 3A, left). A bifurcation diagram as such is said to have a *cone structure* in a small neighborhood of the origin (we recommend [27] for a more detailed discussion).

There exist a few types of DBT singularity. We choose the focus case under time reversal, and this determines the signs of the terms in Eq. 1 as described in [14]. This type hosts the greater variety of behaviors and is able to support more bursting types [36]. Eq. 1 gives a manifold of fixed points (Fig. 2A) in which the upper branch is always stable, while fixed points on the lower branch can destabilise through a Hopf bifurcation, so that oscillations can surround them. Such a configuration is suitable, for example, to build bursting systems in which the active oscillatory phase is at a lower value of x, as it can be observed during seizure-like events [23]. On the other hand, bursting in single neurons is typically characterized by a higher valued oscillatory phase. This can be achieved by applying the

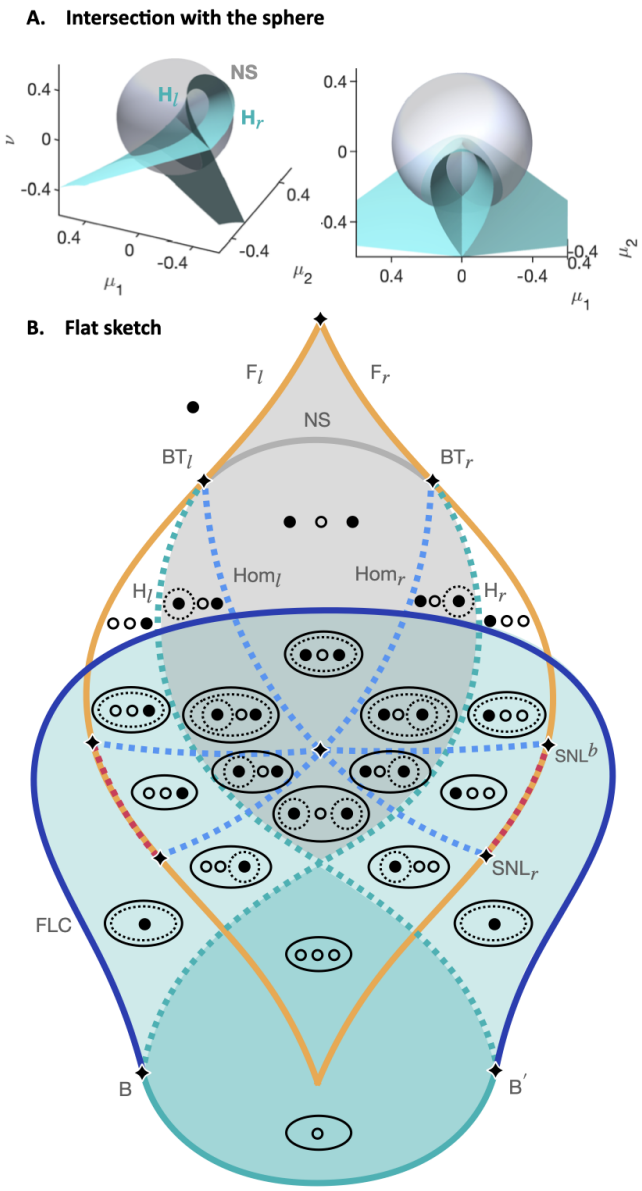

Fig. 4 Unfolding the symmetric case on the sphere (b=0). A. Intersection between the $trace(J) = 0$ manifold of Hopf and Neutral-Saddle and the sphere. **B.** Flat sketch of the bifurcation topology. Modified from [25]. Legend as in Fig. 2.

transformation $x \to -x$ to Eq. 1: now oscillations surround the upper branch. This is still the focus case, time reversal. Bifurcation diagrams as those shown in this paper stay unchanged under this scenario, while the state space representation for each region needs to be flipped.

Case $b = 0$: unfolding the symmetric case

When $b = 0$, the bifurcation diagram has a cone structure in the full space [25]: bifurcation diagrams on spheres are topologically equivalent for any value of R (Fig. 3A, right). This bifurcation diagram is the main focus of [25]. We refer to it as the "symmetric" case (Fig. 4).

Intermediate cases in the literature

When fixing a positive $b = b^* > 0$, for $R > R^*$ we encounter bifurcation diagrams with different topologies. If the topology changes, we have transitioned to a different *case*. The conjecture is that, for big enough radii, this sequence of intermediate cases leads to the topology of the symmetric one, case (a) in this paper (Fig. 3B, top). This approach is used in [27], which, starting from a small radius yielding the unfolding of the DBT (in this paper, case (m)), provided numerical results for the subsequent five cases when increasing R, (cases (l), (k), (i-j*), (h), and (g) in Fig. 5).

Equivalently, we can instead fix the radius $R = R^* > 0$ and vary b. In this case, we find the bifurcation diagram of the unfolding of the DBT (Fig. 2) when b is big enough, and the symmetric case (Fig. 4) when $b = 0$. For intermediate values of b, the bifurcation diagram goes through the sequence of topologically different cases connecting the two extremes (Fig. 3B, bottom). This is the approach we use here.

It is important to note that, because the bifurcation diagram of the intermediate cases lacks cone structure, the exact sequence depends on the type of convex surfaces (spheres, parallelepipeds, ...) chosen to explore the unfolding [27].

2 Results

2.1 Exploring with spheres

2.1.1 A sequence of bifurcation diagrams linking the symmetric case to the DBT one

We are not aware of a lower bound for R that ensures we reach the topology of the symmetric case when using spheres of different radius and fixed b to explore the unfolding, which is the typical approach in the literature. Instead, we know that for $b = 1$, the DBT case can be found on spheres with $R < 0.5$ [36], while the symmetric case occurs as usual for $b = 0$. We thus consider a fixed spherical surface centered around the origin in the $(-\mu_1, \mu_2, \nu)$ space and with $R = 0.4$. We numerically explore the sequence of bifurcation diagram topologies that can be found on it with $b \in [0, 1]$, connecting the symmetric to the DBT case.

Results are sketched in Fig. 5. To avoid confusion with the cases conjectured in [25] and the cases in [27], we labeled them in lowercase.

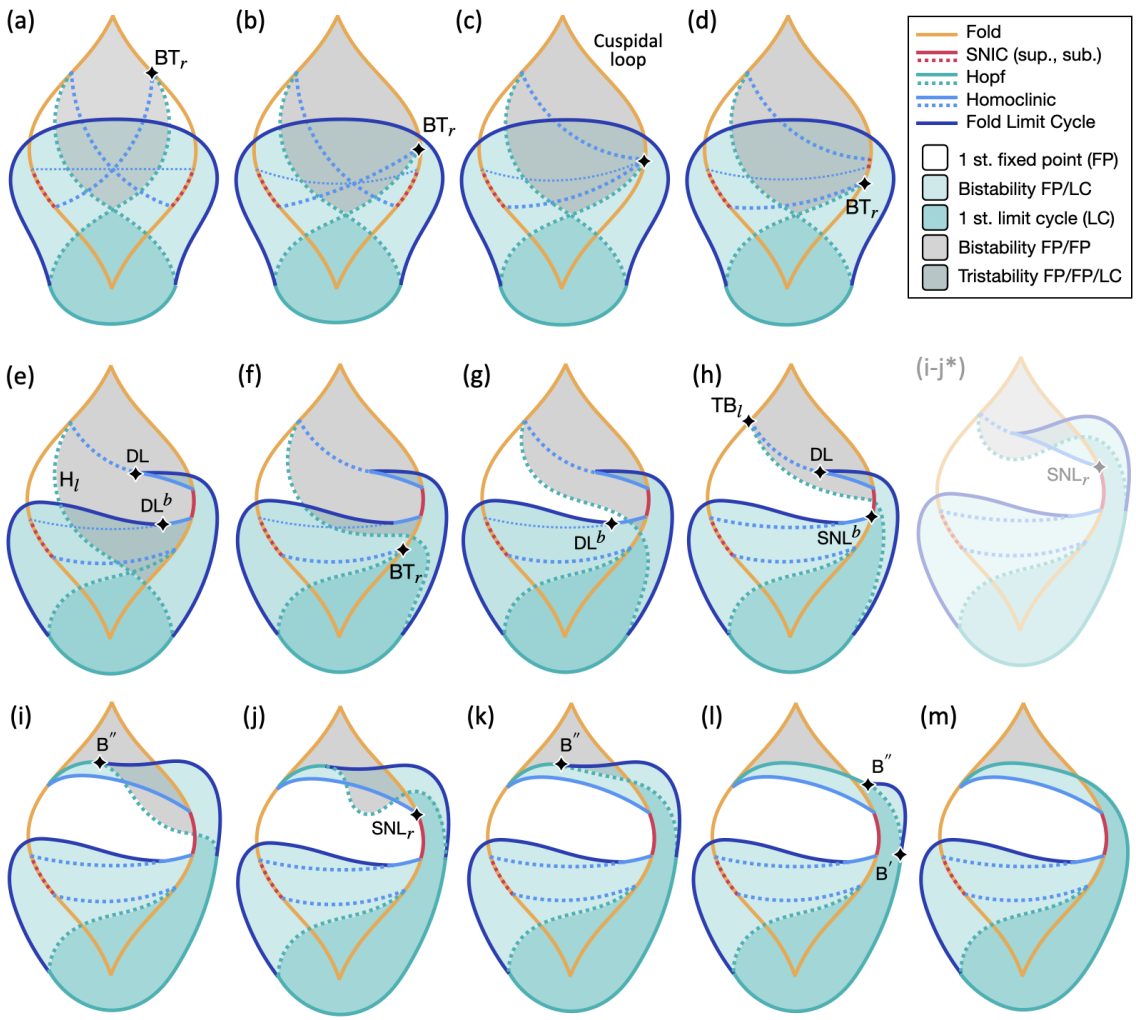

Fig. 5 Varying b enables transitions between symmetric and DBT cases. When increasing b, the bifurcation diagram on the sphere loses the symmetry of the $b = 0$ case and undergoes further modifications as bifurcation curves and points change their relative position with respect to one another. Topologically equivalent diagrams obtained for consecutive steps of b are grouped together in one "case". In each case, we mark with a black diamond the cod-2 points involved in the transition to neighboring cases, and report their label. The colored background highlights how the regions allowing for different attractors deform during the transition. Those shown are sketches, as explained in Fig. 2. The b parameter doesn't alter the fixed points manifold (even though the stability of the solutions can change), nor the fold one, while the other curves are affected. A more detailed version of this figure, with information for attractors and repellors in each region, is shown in Fig. 12. case (i-j*), reported in [27], was here replaced by (i-j). The Hom^b curve, when thinner, is not obtained numerically but based on [25] or consistent with neighboring cases.

We obtained the curves numerically, as detailed in Materials and Methods. We didn't compute the Hom^b curve for cases (a-d). For these cases, we placed this curve according to the literature and consistently with the rest of the diagram, and we drew it thinner in Fig. 5.

The symmetric case (a) has been studied, also numerically, in [25]. Subsequent cases occur when the diagram loses symmetry and curves change their relative position. Along these transitions, the values of b at which cod-1 curves and cod-2 points coincide, and separate two different cases, mark "cod-one-plus-two", that is cod-3, events [27].

cases (b-c) prove to be in accordance with the conjectured (B-C) in [25]: as b increases, the diagram loses symmetry with BT$_r$ moving down. BT$_r$ meets FLC (a cod-3 BT+FLC bifurcation) and then moves below it, giving the new topology in (b). When BT$_r$ coincides with the right extremes of the other homoclinic curves (a cod-3 *cuspidal loop)*, we have the transition to (c). This latter event has been proven in [25].

Between cases (d-e) we observe the FLC curve breaking in two parts, creating two Degenerate-Loop (DL) points, one with Hom$_l$ and the other with Hom^b. In [25] these transitions (D-G in their paper) imply the appearance of a second FLC curve connecting the two

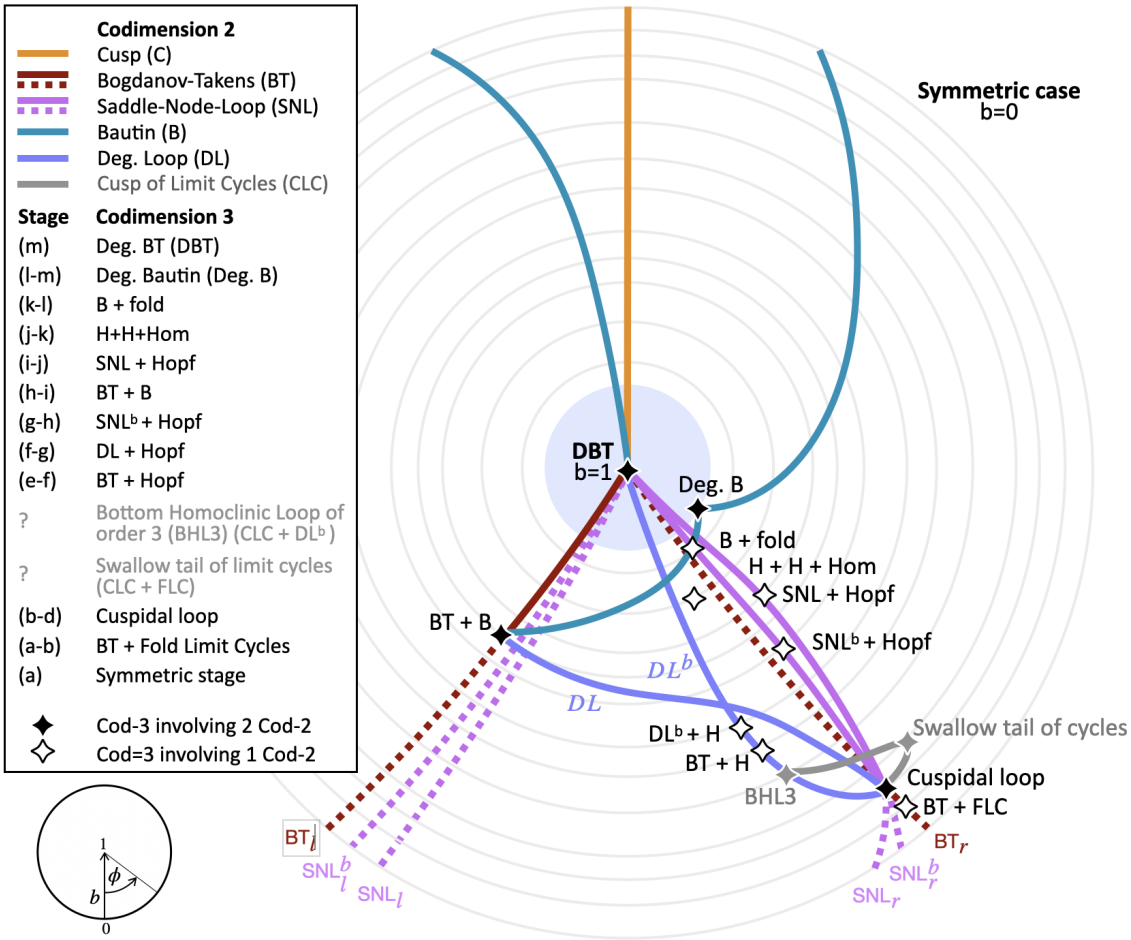

Fig. 6 The cod-4 DDBT organizes lower-order bifurcation curves for varying b. Sketch based on the numerical results. Each radius corresponds to a value of b, with $b = 1$ at the center and $b = 0$ at the outer circle. For each b, we consider the ϕ spherical coordinates of cod-2 points on the full spherical surface and plot them on the circle. We can follow how cod-2 curves persist, appear and disappear when varying b. Diamonds mark cod-3 bifurcations. A light blue background shows the neighborhood of the DBT point where the cone structure is preserved. For the breaking of the FLC curve, we only report the two main events of the conjecture in gray.

homoclinic ones (through DL points) and containing a cusp of limit cycle. As we only continue FLC curves from B points, we cannot confirm this mechanism. However, the behavior of our lower FLC branch after the breaking is different from what is entailed by the conjecture, as it doesn't show any Cusp of Limit Cycle (CLC) bifurcation on it. From this numerical exploration, it appears, however, that the secondary effects associated with the breaking of the FLC curve subside before case (e).

Once the FLC curve has split in two, in (e), the next transition are caused by H_l going above BT_r in (f). These cases, which have not been proven before, differ from the conjecture due to the lack of the CLC. case (e) relates to the conjectured (G), while (f) is implicit in [25].

The following topologies link back to the work of [27], in which cases equivalent to (g-l) lead to the final DBT case (m). The exceptions are (i-j), which are absent in [27]. In the latter work, the transition between (h) and (k) occurs differently, as we show in (i-j*). To corroborate our results, we performed the numerical continuation for these cases also considering a fixed $b = 1$ and varying radius, and confirmed, for this choice of parameters, the occurrence of (i) and (j).

We now describe (g-l) in more detail. In (g), H_l moves above DL^b, and above SNL^b in (h). Here, between (h) and (i), DL and BT_l coalesce. This brings to (i) in which H_l and Hom_l are inverted, and DL disappeared, replaced by B''. This transition occurs through a cod-3 $BT + B$ bifurcation.

In (j), H_l moves above SNL, with a portion of it still below Hom_l. H_l is fully above Hom_l in (k).

Lastly, B'' moves rightward of F_r in (l), before the FLC curve disappears, through a cod-3 *deg. Bautin*, leading to (m).

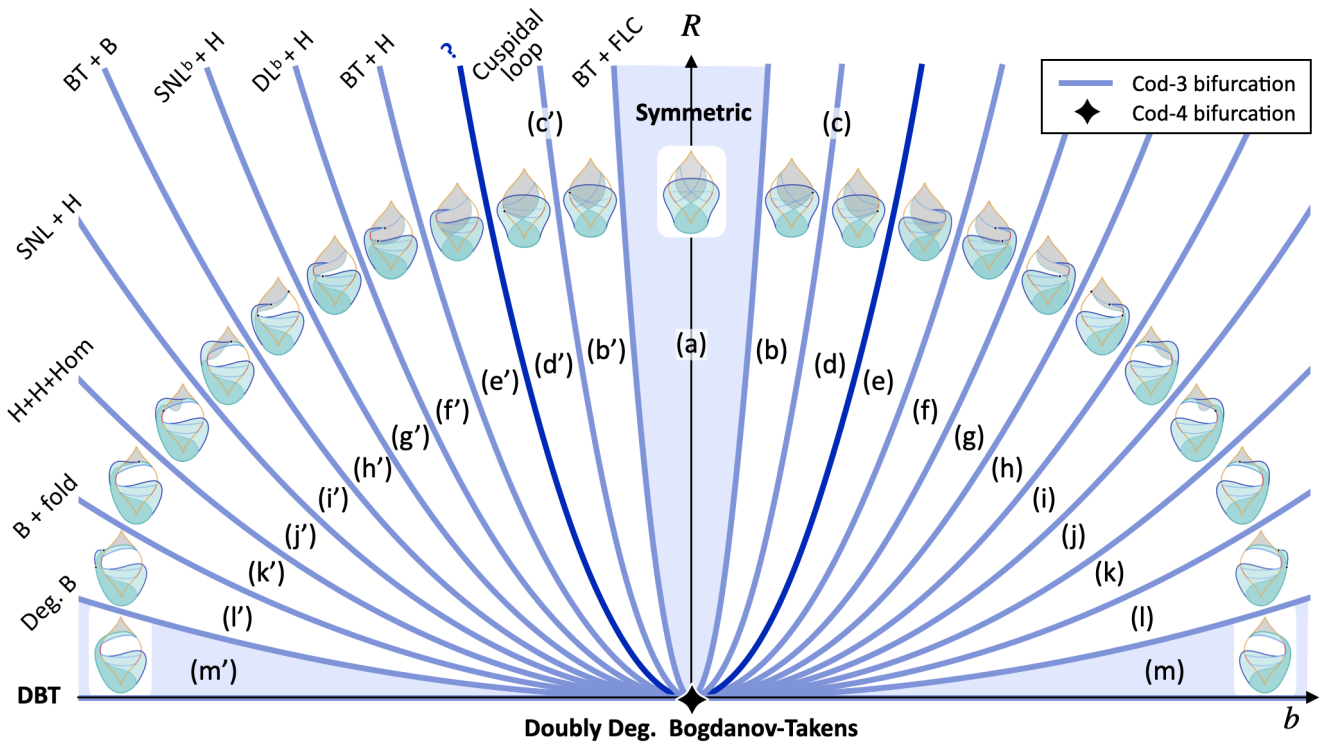

Fig. 7 The unfolding of the DDBT point. The DDBT singularity is at the origin of the four-dimensional parameter space $(-\mu_1, \mu_2, \nu, b)$. We can visualize its unfolding by representing $(-\mu_1, \mu_2, \nu)$ collectively through the radius R of a sphere centered at the origin of the three-dimensional space. Each point in the (b, R) plane then corresponds to the bifurcation diagram on a sphere of radius R for a given value of b. Cod-3 bifurcation curves (light blue) stem from the DDBT point and partition the space into the different cases linking the unfolding of DBT to the symmetric topology. For positive b, the sequence is as shown in Fig. 5, while the topologies are flipped for negative b (represented here with a prime). A question mark reflects our incomplete knowledge about the transition from (d) to (e), involving the breaking of the FLC curve. The cod-3 bifurcations involved are represented together with a darker blue curve. The symmetric case has cone structure because the same topology persists for all values of R (light blue, middle). The unfolding of the DBT has cone structure in a neighborhood of the origin in $(-\mu_1, \mu_2, \nu)$ space (light blue, bottom). The size of this neighborhood decreases with smaller $|b|$. Taking a vertical line corresponds to exploring the unfolding through spheres of different radii and fixed b, while a horizontal one is the approach used here, with a fixed radius and varying b. Applying the method of concentric spheres to investigate this cod-4 unfolding would translate to studying concentric half-circumferences in this (b, R) plane. This figure is a sketch, not based on a detailed numerical exploration of the full space.

If b, instead, decreases from 0 to -1, the sequence appears mirrored along the vertical axis, with BT_l moving below FLC and so on.

2.1.2 The unfolding of the cod-4 DDBT and how it organizes cod-3 curves

We provide two new visualizations for a deeper and cohesive understanding of the several cases and transitions among them.

We can describe how cod-3 and cod-2 vary with b by plotting, for each value of b, the values of the spherical coordinates ϕ of the cod-2 points found on the sphere. We then consider the radius of the plot to correspond to different values of b, from $b = 1$ at the center, to $b = 0$ for the outer circle. This allows us to see, for each b , which cod-2 bifurcations exist and how they persist for close values of the parameter. The result is presented in Fig. 6. Cod-3 events break the conic structure in the neighborhood of the DBT point (light blue background) and gradually lead to the symmetric case.

The unfolding of the cod-4 DDBT, on the other hand, can be sketched by describing the three parameters $(-\mu_1, \mu_2, \nu)$ through the radius R, and drawing the (b, R) space (Fig. 7). Here, each point is a spherical surface and we can observe how the topology of the bifurcation diagram on it varies through the space, as dictated by the cod-3 bifurcation curves stemming from the DDBT point.

2.2 New topologies found using planes

While closed surfaces, such as spheres, allow for a systematic exploration of the unfolding, in applications we often deal with slices of parameter space (see, for ex-

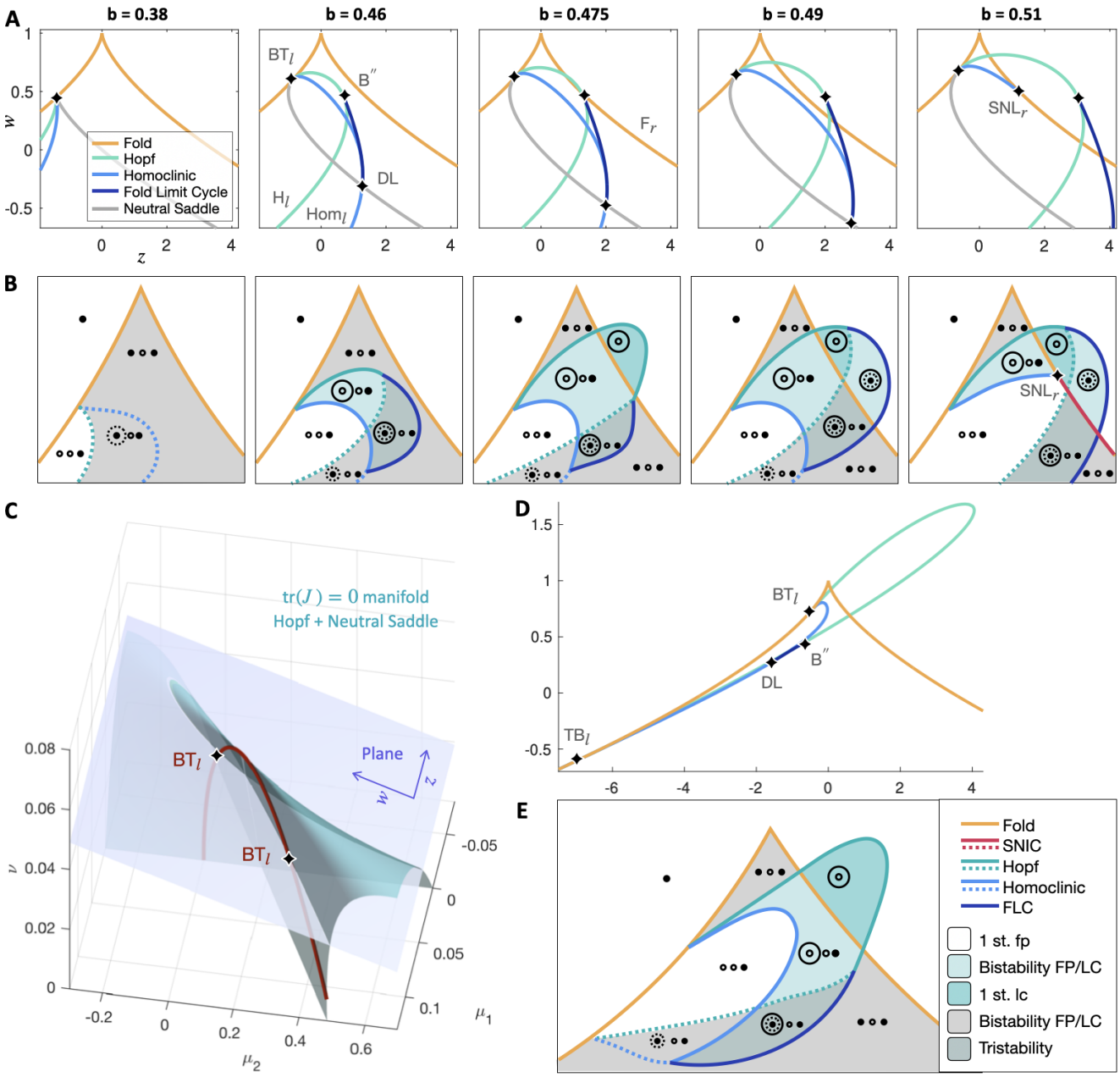

Fig. 8 New topologies of bifurcation diagrams found on planes. A. We considered a plane in the $(-\mu_1, \mu_2, \nu)$ unfolding parameter space, parametrized by the two vectors **z** and **w**. When changing b, the bifurcation diagram includes topologies that are not found on spheres. The transition between the first and second panels is reminiscent, close to BT_l, of that between cases (h) and (i), where Hopf and homoclinic curves invert. However, the bifurcations involving limit cycles remain confined between fold curves. In the third panel the B point moves to the right of F_r and in the last panel Hom_l terminates in SNL_r rather than DL. For these plots $\nu_{P_3} = 0.08$. **B.** Sketches topologically equivalent to the corresponding bifurcation diagram of panel A. We include information about state space configuration. **C.** A 3D view showing how some planes can intersect the same cod-2 curve, here BT_l, more than once. **D.** Bifurcation diagram on the plane for the situation of panel C. **E.** Topologically equivalent sketch.

ample, [6,19]). We thus investigated whether planes can host bifurcation diagrams with topologies not found on spheres.

Using concentric spheres, we can study the three-dimensional space $(-\mu_1, \mu_2, \nu)$ by changing the radius R. With planes, instead, we have more possibilities. In this work, we focused on planes crossing the line of cusp bifurcations at a positive value of ν (in Fig. 2B, top, this corresponds to the top cusp point), motivated by the fact that many models of neural dynamics display bistability between fixed points, corresponding to up and down states. We parametrized a plane through

three points $P_1 = (0, 0.2, 0)$, $P_2 = (-0.01, 0.2, 0)$ and $P_3 = (0, 0, \nu_{P_3})$. The two coordinate vectors on the plane are thus $\mathbf{z} = \overline{P_1P_2}$ parallel to μ_1, and $\mathbf{w} = \overline{P_1P_2}$ perpendicular to μ_1. The parameter ν_{P_3} determines how far from the middle of the sphere the cusp point is on the plane in $(-\mu_1, \mu_2, \nu)$ space. However, because of how we defined the plane vectors, the cusp in the plane coordinates is always at $(z, w) = (0, 1)$. This simplifies our numerical analysis and puts the focus on topology.

Interestingly, for different values of ν_{P_3} we find a range of b values for which the bifurcation diagram on the plane is topologically different from those we computed on spheres, as shown in Fig. 8A,B for $\nu_{P_3} = 0.08$. This is due to the H and/or Hom_l curves stemming from BT_l bending back towards F_l because of how the plane intersects the cod-1 bifurcation manifolds.

The bending back of the curves is stronger for smaller values of ν_{P_3} and less pronounced for bigger ones. For small ν_{P_3}, we can however always find a range of b producing these topologies.

Another consequence of this bending is that, on planes, we can cross the BT_l manifold twice. An example is shown in Fig. 3C-E.

3 Discussion

It has been conjectured that the unfolding of the cod-4 Doubly Degenerate Bogdanov-Takens singularity (DDBT) connects the symmetric bifurcation diagram studied in [25] to that of the codimension-3 degenerate Bogdanov-Takens singularity (DBT) through a number of intermediate topologies. Some conjectured cases of the transition, those closer to DBT, have been modified after numerical exploration by Krauskopf and Osinga [27]. We here expand on that work and provide a numerical evaluation of other cases of the transition. We perform this exploration using the intersection between each bifurcation manifold and the surface of a sphere centered at the origin of a three-dimensional parameter space, while the fourth parameter is allowed to vary. In addition, we show that different topologies of bifurcation diagrams arise when the unfolding is studied through planes.

Concerning the diagrams obtained on spheres, our results are consistent with those of [27] for the cases closer to DBT, with the replacement of case (i-j*) with two other unreported ones. We go further and connect these bifurcation diagrams to the symmetric one as conjectured. New cases include (e-g), differing from the conjecture for the lack of the Cusp of Limit Cycle bifurcation.

The main limitations of our work with spheres are that: we did not attempt the continuation of the Hom^b curve when the DL^b point disappeared (cases (a-d) in our sketches); and we only continued FLC curves from Bautin points. These limitations constrained our understanding of the FLC breaking mechanism.

The passages involved in the FLC curve breaking (cases (c-e)), thus, remain a missing piece in the puzzle. In our numerical exploration, however, we don't see the secondary effects of the conjectured mechanism [25], such as the presence of CLC bifurcations, beyond case (d). This extends the observations of [27] to earlier cases. It is interesting to note, however, that a CLC appears in the bifurcation diagram of a well-known neural mass model, the Jansen-Rit model [22] (see Fig. 4 in [37]), for which the DBT bifurcation has been identified. The CLC enables a distinctive feature of this model, that is the coexistence of limit cycles with different amplitudes. A point where fold, FLC and homoclinic are said to co-occur, on the other hand, can be found in the detailed analysis of another established model, the Morris-Lecar [31], this time at the single neuron scale ([38], Fig. 4). A clarification of the FLC breaking, and the conjectured link between the CLC and the DDBT unfolding, will improve our understanding of such models. Even though the study of this transition will require more finely tailored numerical approaches than those of the current work, our results constrain these events to a precise range of b values. More details about the conjectured FLC breaking and our partial numerical results for it can be found in Fig. 9.

Another factor that makes the analysis difficult is that some of the bifurcation curves are very close (see, for example, Figs. 10 and 9). This proximity among curves could be the reason behind the discrepancies between (i-j) and the analogous case reported in [27]. Further elucidations could be obtained by repeating the analysis on spheres of different radii. We tried this for $b = 1$, which corroborated our results Fig. 10, but a more systematic search could identify parameter values for which bifurcation curves are even more resolved.

Despite the limitations, the intermediate cases expand our understanding of models organized by the DDBT singularity. For example, the already mentioned Morris-Lecar model, in its biologically relevant parameter range, has a bifurcation diagram, as shown in Fig. 6 of [20], equivalent to case (h) of the current paper. This suggests that transitions to neighboring cases are possible under parameter variation. It would be interesting to explore if this occurs within physiological (or possibly pathological) parameter ranges and what the implications for the neuron's behaviors would be. (h), in fact, is a particular case, together with (i), in which excitable behavior close to SNIC, that is Type I neuronal excitability, can occur with or without coexistence

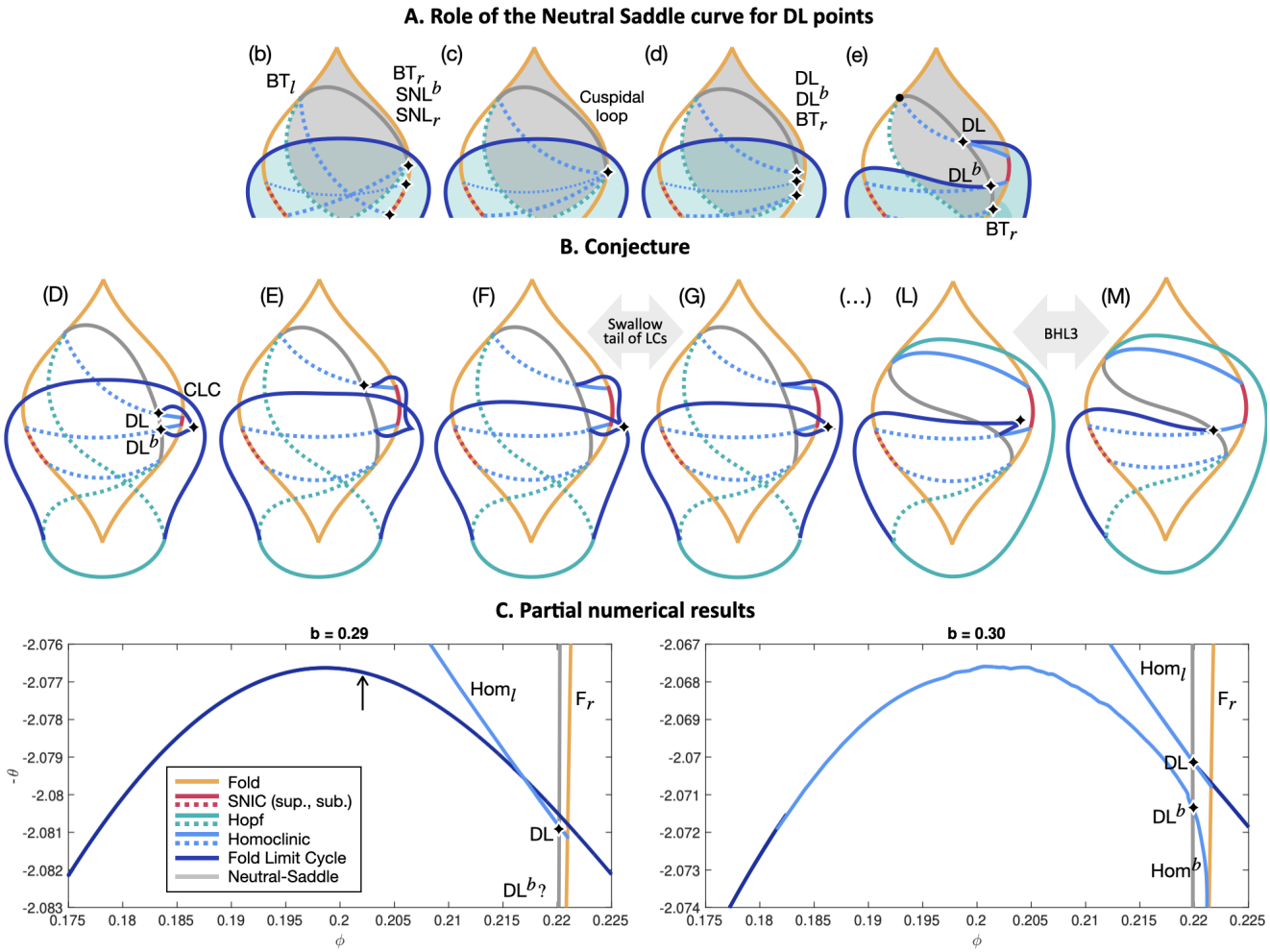

Fig. 9 The breaking of the FLC curve. A. At a DL point, the homoclinic curve changes from being subcritical to supercritical or vice versa. This occurs when the saddle fixed point becomes a *neutral saddle*, that is, when its *saddle quantity* (the sum of its two real eigenvalues) is zero. DL bifurcations, as found in cases (e-l), thus occur at the intersection between the NS curve and the Hom curves. These intersections only exist when BT$_r$ moves below the SNL points, after (c). **B.** The conjecture [25] proposes that a FLC curve joining the two DL points contains a CLC. This gives a limit cycle of multiplicity four when it intersects the old FLC curve (F). This is unfolded by a swallow tail of limit cycles, allowing the breaking of the FLC curve, and leaves a CLC on the lower branch which persists until case (L). Adapted from [25]. **C.** Numerical results in the parameter range where we observe the breaking of the FLC curve. SNL^b from DL^b was not computed in the left panel. An arrow points to where the FLC branches partially overlap in the numerical results. While we cannot confirm or not the presence of the new FLC curve and its transitions, two differences from the conjecture already appear: SNL seems to be below FLC when the curve breaks; no CLC is detected on the broken FLC branches.

with another fixed point (grey or white background in Fig. 5 respectively). In close cases, only one of these two possibilities persists.

The presence of case (h) in the Morris-Lecar neuron model provides another source of support, in addition to pseudo-plateau bursting [33], for the need to consider the full cod-4 unfolding to understand neural dynamics.

In addition to spheres, we also use planes to explore the unfolding (Fig. 8). This leads to new topologies due to the inward bending of the Hopf and related bifurcation curves. The extreme scenario involves bifurcation diagrams with two BT$_l$ points. In this scenario, the SNIC segment on F$_r$ can be preserved, when Hom$_l$ reaches F$_r$, as in [33]. The SNIC segment is instead lost, and thus the possibility of excitable behaviors close to it, if Hom$_l$ bends back earlier, as shown here. Diagrams of this type, with two BT points on the same fold branch, have been observed in the neural dynamics literature, for example, in the Wilson-Cowan neural mass model [41,8].

The use of planes is exploratory rather than systematic, and other topologies may be possible that we did not identify. As mentioned above, the SNIC segment on F$_r$, present in cases (e-m), is usually associated with Type I neuron excitable behavior in single neuron models. Changing the parameters to reach lower por-

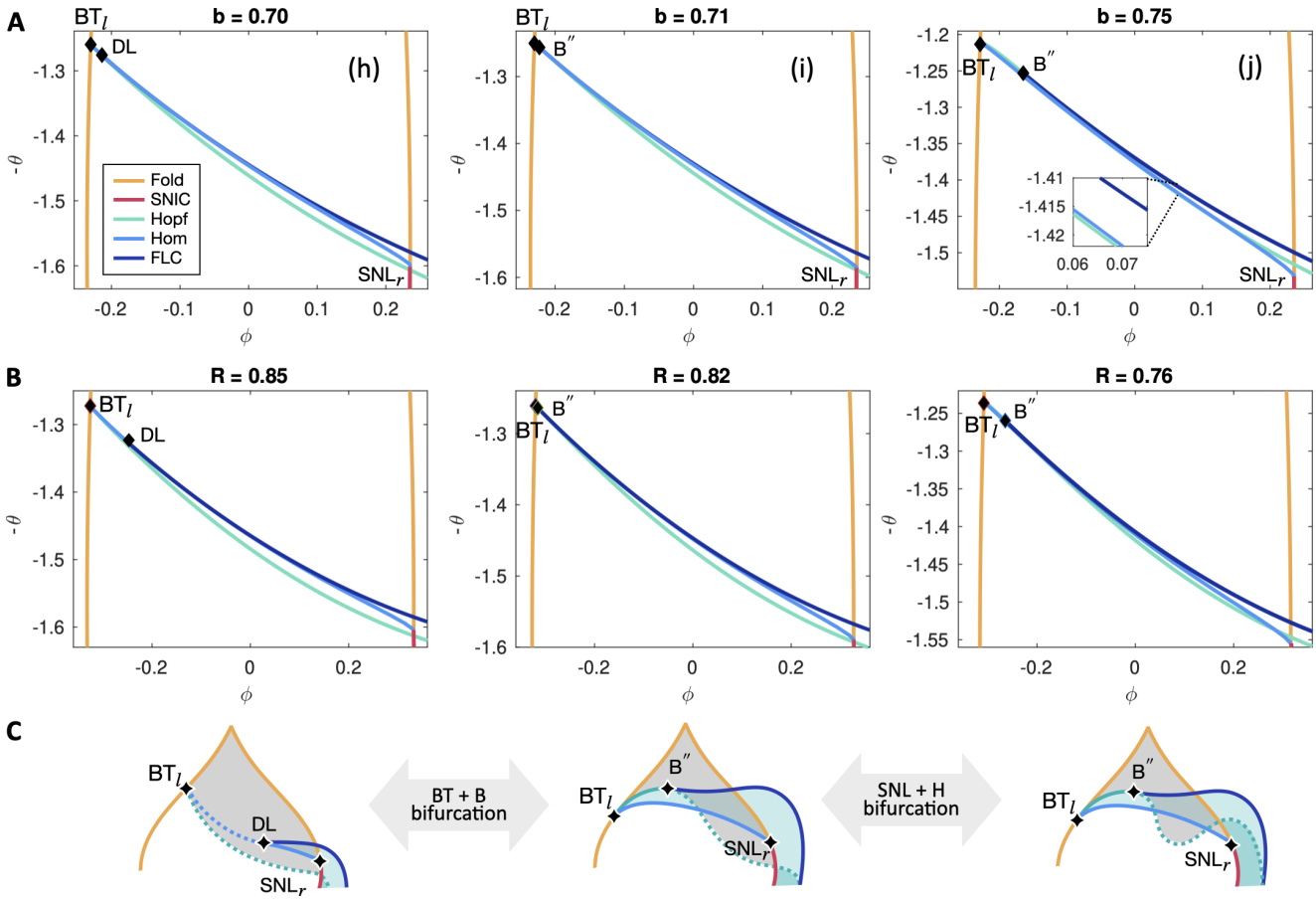

Fig. 10 New cases in the transition from (i) to (l). We show numerical continuation results for cases (h-j).**A.** Results for fixed $R = 0.4$, ad in the rest of the manuscript. In (i), the Hopf curve stemming from BT_l stays below the Hom_l curve. In (j), the first portion of H is above Hom_l and forms a Bautin point with FLC, it then passes below Hom_l. In (k), H behaves as in (j), except going above Hom_l again before the latter disappears in SNL_r. **B.** The same cases can be found by fixing b (here $b = 1$) and varying the radius. **C.** Sketch of the topologies.

tions of the unfolding causes a structured sequence of transitions in neural excitability Type as the system moves beyond cod-2 points [26,1]. Future work will address whether new topologies in the family of planes intersecting the lower Cusp (negative ν_{P_3}) affect these transitions in neuron excitability. We here focused, instead, on planes intersecting the upper Cusp (positive ν_{P_3}), related to transitions in neuron dynamics involving fixed points with different x values, such as up and down states or depolarization block.

Gaining familiarity with the topologies of bifurcation structures allowed by the DDBT unfolding will allow more researchers to recognize the signatures of the presence of this point in their models and gain a deeper understanding of their possible behaviors. In neural dynamics, a wider acknowledgment of the presence of the cod-3 DBT point in models is helping to unify different excitable and bursting behaviors [33,26,36,32]. The topologies provided here will allow further investigation of the role of the fourth parameter of the DDBT in systems, also beyond neuroscience, for which DBT singularities have already been identified.

In summary, our results confirm the main conjecture for the DDBT unfolding, restrict the parameter range to be studied to clarify a missing transition, identify new transitional cases, and show that planar sections reveal additional, potentially biologically relevant topologies.

Future work will extend the unfolding theory approach to fast-slow bursting [19] to the DDBT to examine whether the newly identified topologies permit additional bursting patterns.

4 Materials and Methods

We used Matcont version 7p6 [13] command line for numerical continuation.

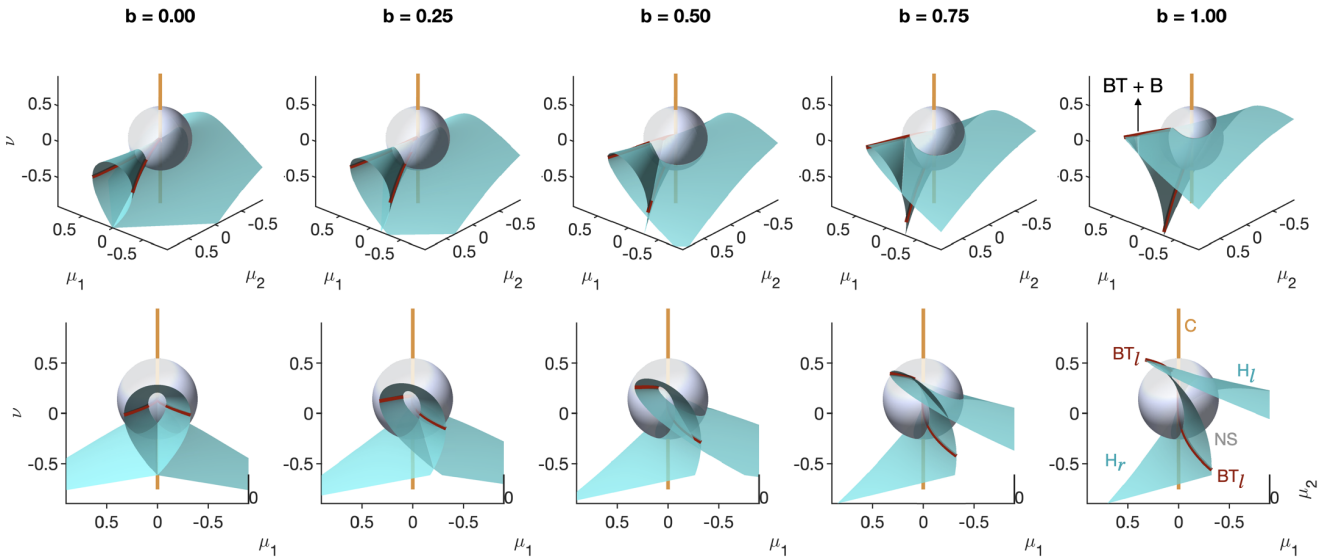

Fig. 11 The Hopf manifold loses symmetry with varying b. For increasing b the manifold corresponding to $trace(J) = 0$, which includes Hopf and neutral-Saddle, loses symmetry. The NS portion, for small b, joins the two BT curves (dark red) on the top. When the cod-3 event "BT + B" is outside the sphere, NS on the spheres joins the two BT points in the middle of the manifold. Two views, lateral (top row) and frontal (bottom).

4.0.1 Bifurcation diagrams on spheres

We expressed the parameters in spherical coordinates as follows:

$$\begin{aligned} \mu_1 &= -R\sin(\theta)\sin(\varphi) \\ \mu_2 &= \quad R\sin(\theta)\cos(\varphi) \\ \nu &= R\cos(\theta) \end{aligned} \tag{2}$$

and replaced Eq.2 in Eq.1. We fixed $R = 0.4$ based on previous work [36].

The fold manifold does not depend on b, so its intersection with the sphere remains as in Fig. 2C (analytical results). The Hopf manifold, instead, is symmetric for $b = 0$ and loses symmetry while b increases (Fig. 11, analytical results).

For the numerical exploration, we used $b \in [0, 1]$ with step 0.02.

We initialized the system in the upper cusp, which can be shown analytically to occur for $(x, y) = (0, 0)$ and $(\theta, \phi) = (0, 0)$. We continued the fold curve (LP in Matcont), on which the two BT points were identified. From the BT points, we continued the Hopf (forward and backward) and homoclinic curves. If the Hopf curve had Bautin points (GH in Matcont), we continued FLC (LPC in Matcont) from there. We also followed homoclinic curves from the end point of the FLC ones to reconstruct Hom^b for cases from (e) onward. This was the most delicate continuation, which sometimes failed. We reconstructed this full curve at least once within a given case, except in (e-g), where the subcritical branch is placed according to subsequent cases, while the supercritical branch is numerical. We did not reconstruct this curve before the breaking of the FLC curve. In those sketches, Hom^b is based on the literature, with that in (a) verified numerically in [25].

Our algorithm computes some curves several times (for example, forward and backward Hopf branch from the two BT points coincides, so as the Bautin points on them from which we continued FLC curves, and so on). A minimal implementation would be: from the the cusp continue folds. Continue homoclinic curves from both BT points, but Hopf from only one of them (backward and forward). Continue FLC curves from all Bautin points on the Hopf curve. Continue the Hom^b from the end point of the lower branch of the FLC curve. However, computing the same curves with different starting points gave robustness to our results, in particular for delicate continuations such as the Hom^b one, so we maintained the redundancies.

We performed exploration at a higher b resolution to resolve transitions among cases when not clear. For the transition between (h) and (k) we used a step of 0.005 for $b \in [0.7, 0.75]$. At this resolution, the transition between (h) and (k) was achieved through two intermediate cases, (i) and (j) (Fig. 10) both different from the single transition case observed in [27] (here (i-j*)). In the latter work, the unfolding was explored by fixing b and varying R. We also tested fixing $b = 1$ and varying $R \in [0.75, 0.85]$, with step 0.01, which yielded again to (i) and (j).

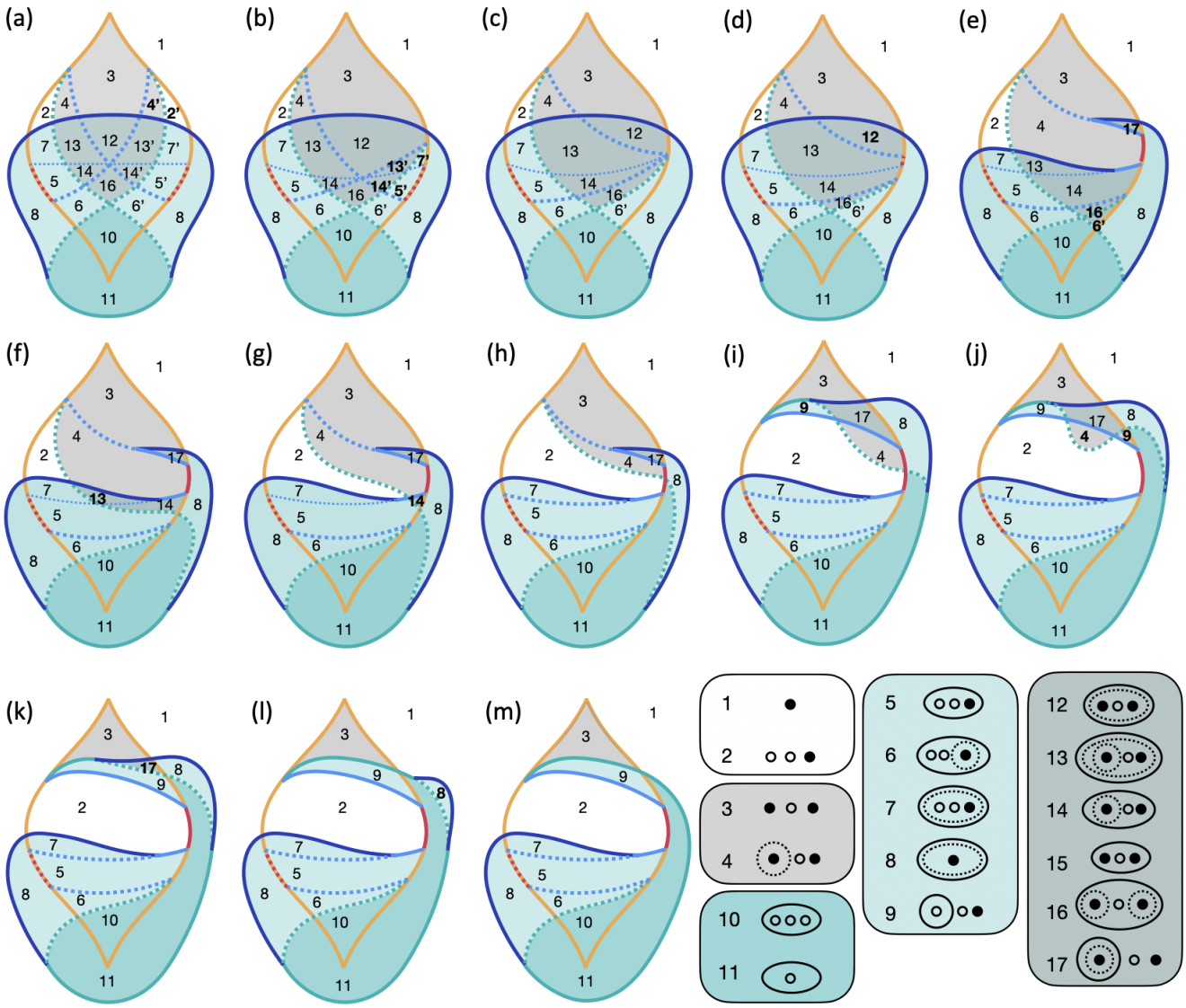

Fig. 12 Transitions with information about state space configuration. This is a more detailed version of Fig. 5, where numbers in each region refer to a specific topology of stable/unstable fixed points (filled/empty dots) and stable/unstable limit cycles (full/dashed ellipses). Bold numbers mark regions appearing or disappearing in the neighboring cases.

For the transition between (d) and (e), where the FLC curve breaks in two, we used a step of 0.005 with $b \in [0.25, 0.32]$. We also decreased step sizes and increased the sensitivity of the numerical continuation for the FLC curve. With this increased sensitivity, however, the numerically computed curve is already broken at $b = 0.25$, with the two branches overlapping. For $b = 0.29$, the two endpoints nearly coincide (arrow in Fig. 9C) and separate for $b = 0.3$. However, one of the two endpoints doesn't coincide with the DL^b point, calling for improved continuation. In general, the FLC curve stemming from B ended before reaching the Neutral-Saddle curve. This may explain our difficulties in continuing the subcritical branch of Hom^b from there.

Examples of b values relative to each case are: (a) $b = 0$, (b) $b = 0.27$, (c) $0.265 < b < 0.27$, (d) $b = 0.28$, (e) $b = 0.32$, (f) $b = 0.34$, (g) $b = 0.48$, (h) $b = 0.64$, (i) $b = 0.71$, (j) $b = 0.75$, (k) $b = 0.8$, (l) $b = 0.9$, (m) $b = 1$.

Fig. 12 provides a more detailed version of the cases, with a sketch of state space for each region.

4.0.2 Bifurcation diagrams on planes

We considered the parametric equations of a plane through three points P_1, P_2, P_3. We chose the points so that the plane would intersect the upper C point. We anchored P_1, P_2 such that $\mathbf{z} = \overline{P_1, P_2}$ would be parallel to the $-\mu_1$ axis and have $\mu_2 = 0.2$. P_3, instead,

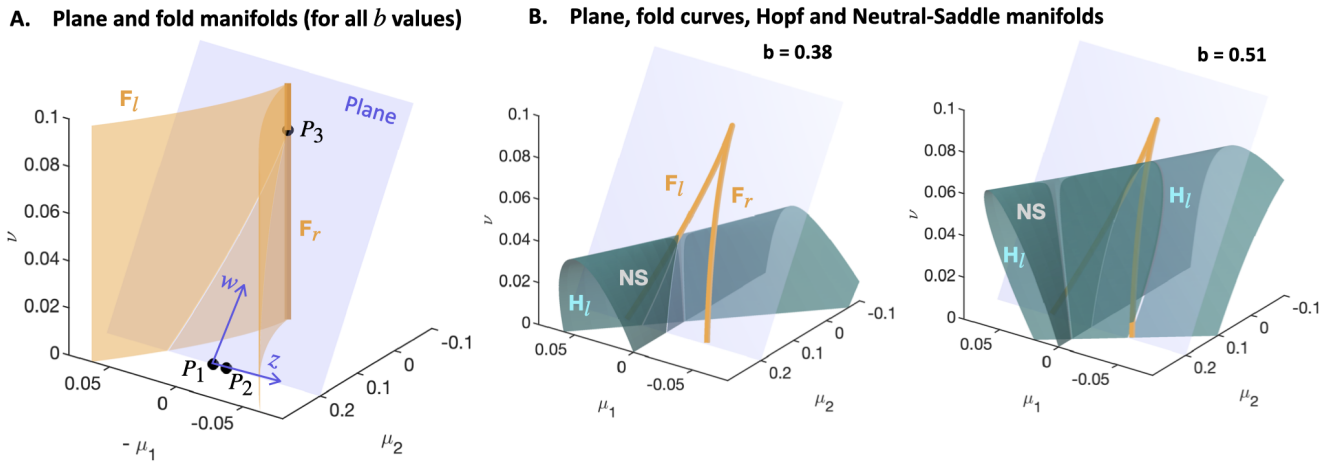

Fig. 13 Construction of the plane and intersections with local cod-1 bifurcation manifolds. A. Plane through three points and intersection with the SN manifold. By construction, this intersection is the same for different values of b and ν_{P_3}. **B.** Intersection with the manifold where the fixed points satisfy $\mathrm{tr}(J_{fp}) = 0$. This manifold represent H bifurcation and NS condition. We show the intersection with the plane for some of the values used in Fig. 8A,B.

lies on the ν axis at $\nu = \nu_{P_3}$. This gives $\mathbf{w} = \overline{P_1 P_3}$ perpendicular to $\mathbf{z}$ and passing through C. We used (z, w) as bifurcation parameters on the plane and we considered different (ν_{P_3}, b) values to study how they affect the bifurcation diagram (Fig. 13).

With our choices $P_1 = (0, 0.2, 0)$, $P_2 = (-0.01, 0.2, 0)$ and $P_3 = (0, 0, \nu_{P_3})$, the plane's parameterization reads:

$$\begin{aligned} \mu_1 &= -0.01z \\ \mu_2 &= 0.2(1 - w) \\ \nu &= \nu_{P_3} w \end{aligned} \tag{3}$$

which we replaced in Eq.1. We initialized the system in the cusp, which can be found analytically to have $(x, y) = (0, 0)$ and $(z, w) = (0, 1)$. From there, we continued the fold curves, identified BT points on them, and continued Hopf and homoclinic curves from BT points. If the Hopf curve had a Bautin point, we continued the FLC curve from there. We did not compute other curves, such as Hom^b, so that we can't locate SNL^b.

Acknowledgements I thank Viktor Jirsa, Jonathan Rubin and Tommaso De Lorenzo for stimulating discussions about this unfolding.

Conflict of interest

The authors declare that they have no conflict of interest.

References

1. Al-Darabsah, I., Campbell, S.A.: M-current induced bogdanov–takens bifurcation and switching of neuron excitability class. The Journal of Mathematical Neuroscience **11**(1), 1–26 (2021)
2. Azim, A.A., Awad, A., Lashin, E.: Degenerate bogdanov–takens bifurcations in a bulk viscous cosmology. The European Physical Journal C **80**(9), 868 (2020)
3. Bautin, A.: Qualitative investigation of a particular nonlinear system: Pmm vol. 39, n. 4, 1975, pp. 633–641. Journal of Applied Mathematics and Mechanics **39**(4), 606–615 (1975)
4. Bazykin, A.: Mathematical biophysics of interacting populations. Nauka, Moscow (1985)
5. Bazykin, A., Berezovskaya, F., Isaev, A., Khlebopros, R.: Parametric foundation of the stability principle ofphytophageentomophage'system dynamics", dokl. Russian Acad. Sci **333**, 673–675 (1993)
6. Bertram, R., Butte, M.J., Kiemel, T., Sherman, A.: Topological and phenomenological classification of bursting oscillations. Bulletin of mathematical biology **57**(3), 413–439 (1995)
7. Boissonade, J., De Kepper, P.: Transitions from bistability to limit cycle oscillations. theoretical analysis and experimental evidence in an open chemical system. The Journal of Physical Chemistry **84**(5), 501–506 (1980)
8. Borisyuk, R.M., Kirillov, A.B.: Bifurcation analysis of a neural network model. Biological cybernetics **66**(4), 319–325 (1992)
9. Bykov, V., Tsybenova, S.B.: Parametric analysis of the simplest model of the theory of thermal explosion—the zel'dovich—semenov model. Combustion, Explosion and Shock Waves **37**(5), 523–534 (2001)
10. Dankowicz, H., Sieber, J.: Computational bifurcation analysis. arXiv preprint arXiv:2411.00735 (2024)
11. De Blank, H., Kuznetsov, Y.A., Pekkér, M., Veldman, D.: Degenerate bogdanov–takens bifurcations in a one-dimensional transport model of a fusion plasma. Physica D: Nonlinear Phenomena **331**, 13–26 (2016)
12. Destexhe, A., Paré, D.: Impact of network activity on the integrative properties of neocortical pyramidal neurons in vivo. Journal of neurophysiology **81**(4), 1531–1547 (1999)

13. Dhooge, A., Govaerts, W., Kuznetsov, Y.A., Meijer, H.G.E., Sautois, B.: New features of the software matcont for bifurcation analysis of dynamical systems. Mathematical and Computer Modelling of Dynamical Systems **14**(2), 147–175 (2008)
14. Dumortier, F., Roussarie, R., Sotomayor, J.: Generic 3-parameter families of planar vector-fields, unfoldings of saddle, focus and elliptic-singularities with nilpotent linear parts (1991)
15. Erisir, A., Lau, D., Rudy, B., Leonard, C.S.: Function of specific k+ channels in sustained high-frequency firing of fast-spiking neocortical interneurons. Journal of neurophysiology **82**(5), 2476–2489 (1999)
16. Ermentrout, G.B., Kopell, N.: Fine structure of neural spiking and synchronization in the presence of conduction delays. Proceedings of the National Academy of Sciences **95**(3), 1259–1264 (1998)
17. Franci, A., Drion, G., Sepulchre, R.: Modeling the modulation of neuronal bursting: a singularity theory approach. SIAM Journal on Applied Dynamical Systems **13**(2), 798–829 (2014)
18. Golomb, D., Donner, K., Shacham, L., Shlosberg, D., Amitai, Y., Hansel, D.: Mechanisms of firing patterns in fast-spiking cortical interneurons. PLoS Computational Biology **3**(8), e156 (2007)
19. Golubitsky, M., Josic, K., Kaper, T.J.: An unfolding theory approach to bursting in fast–slow systems. In: Global analysis of dynamical systems, pp. 282–313. CRC Press (2001)
20. Govaerts, W., Sautois, B.: The onset and extinction of neural spiking: a numerical bifurcation approach. Journal of Computational Neuroscience **18**(3), 265–274 (2005)
21. Izhikevich, E.M.: Neural excitability, spiking and bursting. International journal of bifurcation and chaos **10**(06), 1171–1266 (2000)
22. Jansen, B.H., Rit, V.G.: Electroencephalogram and visual evoked potential generation in a mathematical model of coupled cortical columns. Biological cybernetics **73**(4), 357–366 (1995)
23. Jirsa, V.K., Stacey, W.C., Quilichini, P.P., Ivanov, A.I., Bernard, C.: On the nature of seizure dynamics. Brain **137**(8), 2210–2230 (2014)
24. Khibnik, A., Bykov, V., Yablonskii, G.: 23 phase portraits of the simplest catalytic oscillator. Russian Journal of Physical Chemistry A **61**(5), 722–723 (1987)
25. Khibnik, A.I., Krauskopf, B., Rousseau, C.: Global study of a family of cubic liénard equations. Nonlinearity **11**(6), 1505 (1998)
26. Kirst, C., Ammer, J., Felmy, F., Herz, A., Stemmler, M.: Fundamental structure and modulation of neuronal excitability: synaptic control of coding, resonance, and network synchronization. BioRxiv p. 022475 (2015)
27. Krauskopf, B., Osinga, H.M.: A codimension-four singularity with potential for action. In: Mathematical Sciences with Multidisciplinary Applications: In Honor of Professor Christiane Rousseau. And In Recognition of the Mathematics for Planet Earth Initiative, pp. 253–268. Springer (2016)
28. Kuznetsov, Y.A.: Elements of applied bifurcation theory. Springer (1998)
29. Kuznetsov, Y.A.: Practical computation of normal forms on center manifolds at degenerate bogdanov–takens bifurcations. International Journal of Bifurcation and Chaos **15**(11), 3535–3546 (2005)
30. Medvinsky, A., Adamovich, B., Rusakov, A., Tikhonov, D., Nurieva, N., Tereshko, V.: Population dynamics: Mathematical modeling and reality. Biophysics **64**(6), 956–977 (2019)
31. Morris, C., Lecar, H.: Voltage oscillations in the barnacle giant muscle fiber. Biophysical journal **35**(1), 193–213 (1981)
32. Niemeyer, N., Schleimer, J.H., Schreiber, S.: Biophysical models of intrinsic homeostasis: Firing rates and beyond. Current Opinion in Neurobiology **70**, 81–88 (2021)
33. Osinga, H.M., Sherman, A., Tsaneva-Atanasova, K.: Cross-currents between biology and mathematics: The codimension of pseudo-plateau bursting. Discrete and continuous dynamical systems. Series A **32**(8), 2853 (2012)
34. Prescott, S.A., De Koninck, Y., Sejnowski, T.J.: Biophysical basis for three distinct dynamical mechanisms of action potential initiation. PLoS computational biology **4**(10), e1000198 (2008)
35. Rose, R., Hindmarsh, J.: The assembly of ionic currents in a thalamic neuron i. the three-dimensional model. Proceedings of the Royal Society of London. B. Biological Sciences **237**(1288), 267–288 (1989)
36. Saggio, M.L., Spiegler, A., Bernard, C., Jirsa, V.K.: Fast–slow bursters in the unfolding of a high codimension singularity and the ultra-slow transitions of classes. The Journal of Mathematical Neuroscience **7**(1), 7 (2017)
37. Touboul, J., Wendling, F., Chauvel, P., Faugeras, O., Faugeras Neural mass activity, O.: Neural mass activity, bifurcations, and epilepsy. Neural Mass Activity, Bifurcations and Epilepsy. Neural Computation **23**(12) (2011). DOI 10.1162/NECO_a_00206ï. URL https://inria.hal.science/inria-00592529v2
38. Tsumoto, K., Kitajima, H., Yoshinaga, T., Aihara, K., Kawakami, H.: Bifurcations in morris–lecar neuron model. Neurocomputing **69**(4-6), 293–316 (2006)
39. Vaganov, D., Samoilenko, N., Abramov, V.: Periodic regimes of continuous stirred tank reactors. Chemical Engineering Science **33**(8), 1131–1140 (1978)
40. Wang, X.J., Buzsáki, G.: Gamma oscillation by synaptic inhibition in a hippocampal interneuronal network model. Journal of neuroscience **16**(20), 6402–6413 (1996)
41. Wilson, H.R., Cowan, J.D.: Excitatory and inhibitory interactions in localized populations of model neurons. Biophysical journal **12**(1), 1–24 (1972)